Received: 4 May 2021 | Revised: 31 August 2021 | Accepted: 22 November 2021

DOI: 10.1002/mma.8054

RESEARCH ARTICLE

WILEY

# Time decay for porosity problems

**Jacobo Baldonedo**[1] | **José R. Fernández**[2] | **Ramón Quintanilla**[3]

[1]CINTECX, Departamento de Ingeniería Mecánica, Universidade de Vigo, Vigo, Spain

[2]Universidade de Vigo, Departamento de Matemática Aplicada I, 36310, Vigo, Spain

[3]Departamento de Matemáticas, E.S.E.I.A.A.T., Universitat Politécnica de Catalunya, Barcelona, Spain

**Correspondence**
José R. Fernández, Departamento de Matemática Aplicada I, Universidade de Vigo, Campus As Lagoas Marcosende s/n, 36310 Vigo, Spain.
Email: jose.fernandez@uvigo.es

Communicated by: A. Miranville

**Funding information**
Ministerio de Ciencia, Innovación y Universidades, Grant/Award Number: PGC2018-096696-B-I00 and PID2019-105118GB-I00

In this paper, we numerically study porosity problems with three different dissipation mechanisms. The root behavior is analyzed for each case. Then, by using the finite element method and the Newmark-$\beta$ scheme, fully discrete approximations are introduced and some numerical results are described to show the energy evolution depending on the viscosity coefficient.

**KEYWORDS**

energy decay, finite elements, Newmark scheme, numerical behavior, porosity

**MSC CLASSIFICATION**

74F10; 65M60

## 1 | INTRODUCTION

The theory of porous materials was proposed by Cowin and Nunziato.[1–3] Their intention was to model elastic solids with voids. That is, materials with an elastic matrix where we can find voids of the material. This kind of materials with different damping mechanisms has received a huge attention in the last years (see, e.g.,[4–22]). A good survey of this theory can be found in the book of Ieşan.[23] Different generalizations of these materials have been considered.

Recently, Ieşan[24] has extended the notion of these materials to include strain gradient elastic solids, where the field equation for the porosity contains a fourth-order spatial derivative. Although the elastic effects can be considered, we want to restrict our attention to the case of a rigid porous solid. That is, there are not elastic deformations and we only consider the porosity effects. We believe that it proposes an interesting mathematical problem (also from the physical point of view), because it is a problem where the fourth-order spatial derivative is present and we can introduce different dissipative mechanisms.

The main goal of this paper is to investigate how the different dissipative mechanisms (we can introduce) determine the damping of the solutions. We are in front of an equation of second-order in time variable and fourth-order in the spatial variable. We believe that this can be a physical proposition to investigate a relevant mathematical problem.

The plan of this paper is as follows. In Section 2, we describe the model and we recall an existence and uniqueness result, which can be proved proceeding as in Baldonedo et al.[8] We also discuss the point spectrum of the problem for three dissipation mechanisms: viscoporosity, hyperviscoporosity, and weak porosity. The root behavior is analyzed for each case. Then, using the finite element method to approximate the spatial variable and the Newmark-$\beta$ scheme to discretize

the second-order time derivatives, in Section 3 we present some numerical results for the three dissipation mechanisms. Particularly, we study the dependence of the energy evolution on the porosity parameter.

## 2 | BASIC EQUATIONS

In this section, we describe the evolution and constitutive equations which govern the theory we are going to study, following the ideas proposed by Ieşan.[24]

We will make the assumption that the body is rigid, and so, since our analysis is focused on the one-dimensional problem, the evolution equation is

$$J\ddot{\varphi} = \chi_x - \sigma_{xx} + g.$$

In the previous equation, $\varphi$ is the fraction of volume, $\chi$ is the equilibrated stress vector, $\sigma$ is the equilibrated hyperstress tensor, and $g$ the equilibrated body force. As usual, $J > 0$ represents the product of the mass density by the equilibrated inertia.

The primary constitutive equations are given by

$$\begin{aligned} \chi &= \alpha\varphi_x + \delta^*\dot{\varphi}_x, \\ \sigma &= d\varphi + k_2\varphi_{xx} + k_2^*\dot{\varphi}_{xx}, \\ g &= -\xi\varphi - \xi^*\dot{\varphi} - d\varphi_{xx}. \end{aligned}$$

The conditions for the constitutive coefficients $\alpha,\ d, k_2, k_2^*, \delta^*, \xi$ and $\xi^*$ will be stated below.

Without lost of generality, we suppose that the spatial variable $x$ lies in the interval $[0, \pi]$ and that the time $t$ goes from 0 to $T$, where $T > 0$ denotes the final time.

If we substitute the constitutive equations into the evolution equation, we obtain the following equation:

$$J\ddot{\varphi} = \delta\varphi_{xx} - \xi\varphi - k_2\varphi_{xxxx} + \delta^*\dot{\varphi}_{xx} - \xi^*\dot{\varphi} - k_2^*\dot{\varphi}_{xxxx}, \tag{1}$$

where, to simplify the notation, we set $\delta = \alpha - 2d$.

In Equation (1) we note that we have introduced three dissipation mechanisms: a zeroth-order mechanism related to the term $\xi^*\dot{\varphi}$, a second-order mechanism related to the term $\delta^*\dot{\varphi}_{xx}$, and a fourth-order mechanism related to the term $k_2^*\dot{\varphi}_{xxxx}$.

We point out that, in the previous equation, depending on the value of parameters $k_2^*$, $\delta^*$, and $\xi^*$, we can distinguish three different problems: the viscoporosity problem (corresponding to the case $k_2^* \neq 0$ and $\delta^* = \xi^* = 0$), the hyperviscoporosity problem (corresponding to the case $\delta^* \neq 0$ and $k_2^* = \xi^* = 0$), and the weak viscoporosity problem (corresponding to the case $\xi^* \neq 0$ and $k_2^* = \delta^* = 0$).

The following set of boundary and initial conditions is imposed for all the different systems that we analyze as follows:

$$\varphi(0,t) = \varphi(\pi,t) = \varphi_{xx}(0,t) = \varphi_{xx}(\pi,t) = 0, \tag{2}$$

and, for a.e. $x \in (0,\pi)$,

$$\varphi(x,0) = \varphi_0(x),\ \dot{\varphi}(x,0) = \psi_0(x). \tag{3}$$

Proceeding as in, Baldonedo et al[8] where the coupling with the mechanical effects was also considered, we could prove the following result which states the existence of a unique solution to the above porous problem.

**Theorem 1.** *Assume that the constitutive coefficients satisfy the following conditions:*

$$J > 0,\ \delta > 0,\ \xi > 0,\ k_2 > 0.$$

*Then, there exists a unique solution*

$$\varphi \in C([0,T]; L^2(0,\pi)) \cap C^1([0,T]; H^2(0,\pi)) \cap C^0([0,T]; H^4(0,\pi))$$

*to problem (1)-(3).*

Now, we will analyze the energy decay of problem (1) with boundary conditions (2) and initial conditions (3).

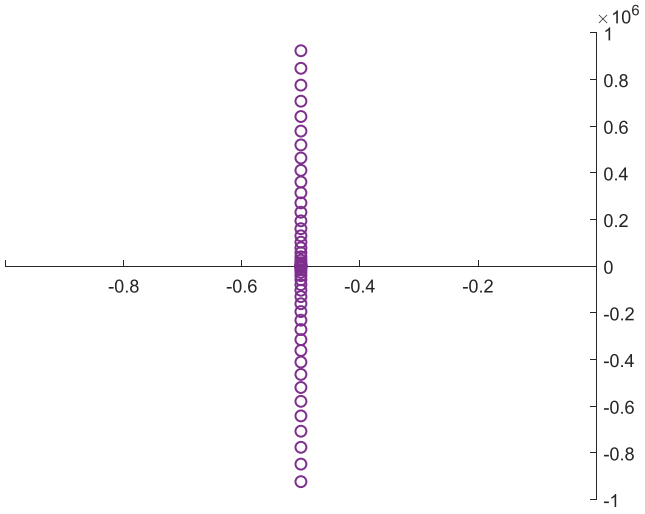


**FIGURE 1** Root's behavior for the weak viscoporosity case [Colour figure can be viewed at wileyonlinelibrary.com]

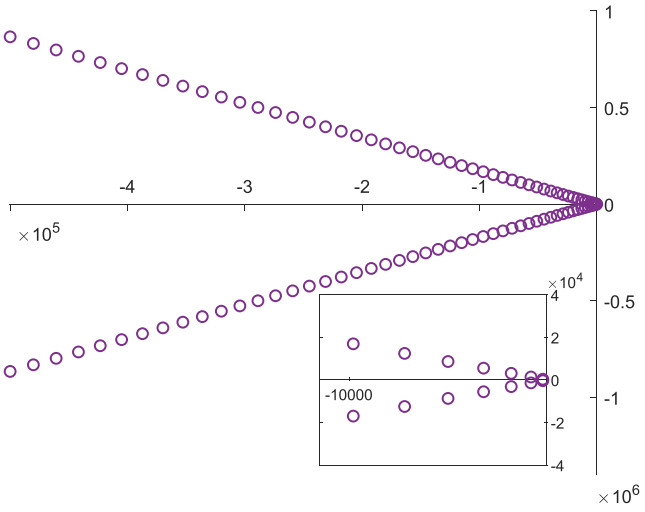


**FIGURE 2** Root's behavior for the viscoporosity case assuming that the term on the square root is negative [Colour figure can be viewed at wileyonlinelibrary.com]

If we suppose the weak viscoporosity case, we obtain the equation:

$$J\ddot{\varphi} = \delta\varphi_{xx} - \xi\varphi - k_2\varphi_{xxxx} - \xi^*\dot{\varphi}.$$

Thus, if we also consider solutions of the form:

$$\varphi(x,t) = e^{\omega t}\sin nx,\ \ n \in \mathbb{N},$$

then it follows that $\omega$ must satisfy

$$J\omega^2 + \xi^*\omega + \delta n^2 + k_2 n^4 + \xi = 0.$$

Therefore, we have

$$\omega = \frac{-\xi^* \pm \sqrt{(\xi^*)^2 - 4J(\delta n^2 + k_2 n^4 + \xi)}}{2J}.$$

Since generally $(\xi^*)^2 < 4J(\delta n^2 + k_2 n^4 + \xi)$, spectrum is bounded because $\mathrm{Re}(\omega) = \frac{-\xi^*}{2J}$, and so, the point spectrum is located on that line.

Taking the particular values:

$$J = 1,\ \delta = 1,\ \xi = 1,\ k_2 = 1,\ \xi^* = 1,$$

in Figure 1 we plot the range of 25 different roots beginning with $n = 1$ and taking an step of $n = 40$ up to $n = 1000$. We find that the point spectrum is located on the line $\mathrm{Re}(\omega) = -\frac{1}{2}$ as expected.

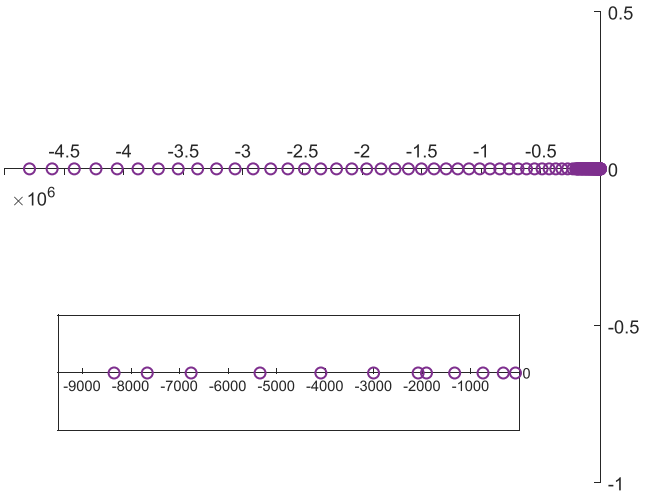


**FIGURE 3** Root's behavior for the viscoporosity case assuming that the term on the square root is positive [Colour figure can be viewed at wileyonlinelibrary.com]

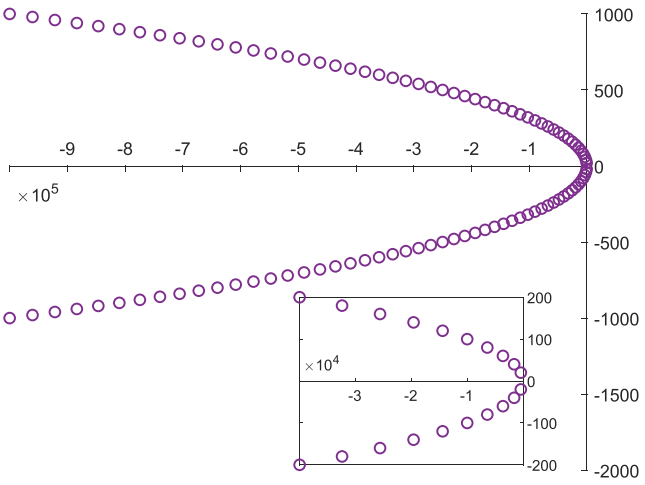


**FIGURE 4** Root's behavior for the viscoporosity case in the limit case $(\delta^*)^2 = 4Jk_2$ [Colour figure can be viewed at wileyonlinelibrary.com]

Secondly, if suppose the viscosity case, it follows now the equation:

$$J\ddot{\varphi} = \delta\varphi_{xx} - \xi\varphi - k_2\varphi_{xxxx} + \delta^*\dot{\varphi}_{xx}.$$

Again, by considering solutions of the form:

$$\varphi(x,t) = e^{\omega t}\sin nx, \;\; n \in \mathbb{N},$$

then we find that $\omega$ must satisfy

$$J\omega^2 + \delta^*\omega n^2 + \delta n^2 + k_2 n^4 + \xi = 0.$$

Therefore, we have

$$\omega = \frac{-\delta^* n^2 \pm \sqrt{(\delta^*)^2 n^4 - 4J(\delta n^2 + k_2 n^4 + \xi)}}{2J}.$$

In the case $(\delta^*)^2 < 4Jk_2$ then the term inside the square root of the previous equation could be negative, and so, its real part would be $-\frac{\delta^* n^2}{2J}$ and the imaginary part would also be of the type $n^2$. In a similar form, if $(\delta^*)^2 > 4Jk_2$, then the term within the square root becomes positive, and so, generally, we will have

$$\frac{-\delta^* + \sqrt{(\delta^*)^2 - 4Jk_2}}{2J} n^2.$$

It implies that the roots would be on the real axis. The limit case $(\delta^*)^2 = 4Jk_2$ leads to a derivation similar to the first case, but now the real part is of the type $n^2$ and the imaginary one of the type $n$.

We take the same particular values as before:

$$J = 1,\ \delta = 1,\ \xi = 1,\ k_2 = 1,$$

but we now show two different cases, depending on the value of the dissipation parameter. In Figure 2, we have taken value $\delta^* = 1$ (so the term within the square root is negative) and we can observe how we have two oblique lines. We also show a zoom around the value $(0, 0)$, and, as can be clearly seen, there is not an accumulation point on that area. In this case, we plot a range of 50 different roots beginning with $n = 1$ and taking an step of $n = 20$ (up to $n = 1000$).

Now, by using the value $\delta^* = 5$ (i.e., the term within the square root is positive) and the same range for parameter $n$, in Figure 3 we plot the roots which, as expected, are almost all negative and real. We can also see a zoom near the point $(0, 0)$ in order to show again that there is not an accumulation point. Moreover, we consider the limit case $\delta^* = 2$ and we show the roots in Figure 4. As in the previous cases, there is not an accumulation point and, as expected, the roots have a quadratic behavior. We can conclude that the nonexistence of an accumulation point constitutes a big difference with respect to the hyperviscoporosity case, where such an accumulation point is found, as we will show below.

Finally, if we suppose the hyperviscoporosity case, we obtain the equation:

$$J\ddot{\varphi} = \delta\varphi_{xx} - \xi\varphi - k_2\varphi_{xxxx} - k_2^*\dot{\varphi}_{xxxx}.$$

Thus, if we also consider solutions of the form:

$$\varphi(x, t) = e^{\omega t}\sin nx,\ \ n \in \mathbb{N},$$

then it follows that $\omega$ must satisfy

$$J\omega^2 + k_2^*\omega n^4 + \delta n^2 + k_2 n^4 + \xi = 0.$$

Therefore, we have

$$\omega = \frac{-k_2^* n^4 \pm \sqrt{(k_2^*)^2 n^8 - 4J(\delta n^2 + k_2 n^4 + \xi)}}{2J}.$$

In the general case, the term within the square root would be positive and so the point spectrum would be close to the value $\frac{-k_2}{k_2^*}$, with almost every root being negative and real.

Finally, we study the third dissipation mechanism, choosing the values:

$$J = 1,\ \delta = 1,\ \xi = 1,\ k_2 = 1,\ k_2^* = 1.$$

In Figure 5 we plot the first 30 roots (from $n = 1$ to $n = 30$). It seems that the point spectrum concentrates around the limit value $\omega = -1$, with almost all the roots laying on the real axis. We can clearly see how an accumulation point is found at the predicted value $\omega = -1$.

From the previous analysis, we see that, in the first case, all the elements in the point spectrum are located at a finite distance of the imaginary axis. In the third case, we see that one branch of the point spectrum is located at a finite distance of the imaginary axis. In the second case, the elements of the point spectrum move away from the imaginary axis. This behavior suggests that the most efficient dissipative mechanism is the viscoporosity, the second more efficient could be the hyperviscoporosity, and the third one corresponds to the weak viscoporosity.

## 3 | NUMERICAL BEHAVIOR

In this section, we study a fully discrete approximation of a variational version of the porosity problems presented in the previous section. So, we introduce its variational formulation. Let $Y = L^2(0, \pi)$ and denote by $(\cdot, \cdot)$ the scalar product in this space, with corresponding norm $\|\cdot\|$.

We replace boundary conditions (2) by the following ones:

$$\varphi(0, t) = \varphi(\pi, t) = \varphi_x(0, t) = \varphi_x(\pi, t) = 0. \tag{4}$$

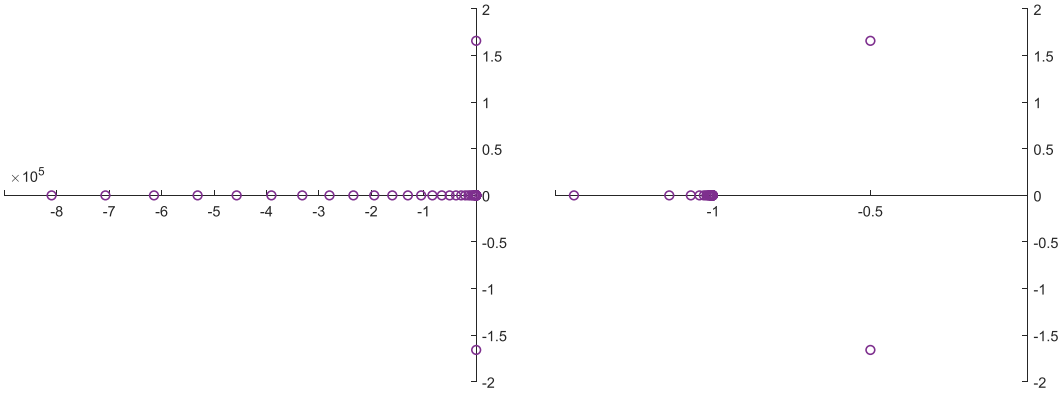


**FIGURE 5** Root's behavior for the hyperviscoporosity case (left) and zoom near zero (right) [Colour figure can be viewed at wileyonlinelibrary.com]

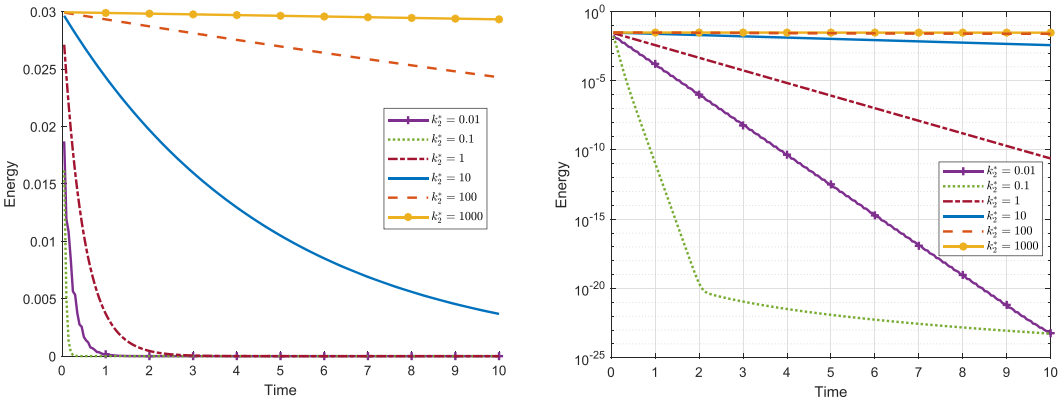


**FIGURE 6** Example 1: dependence of the solution with respect to parameter $k_2^*$ (fourth-order dissipation mechanism) [Colour figure can be viewed at wileyonlinelibrary.com]

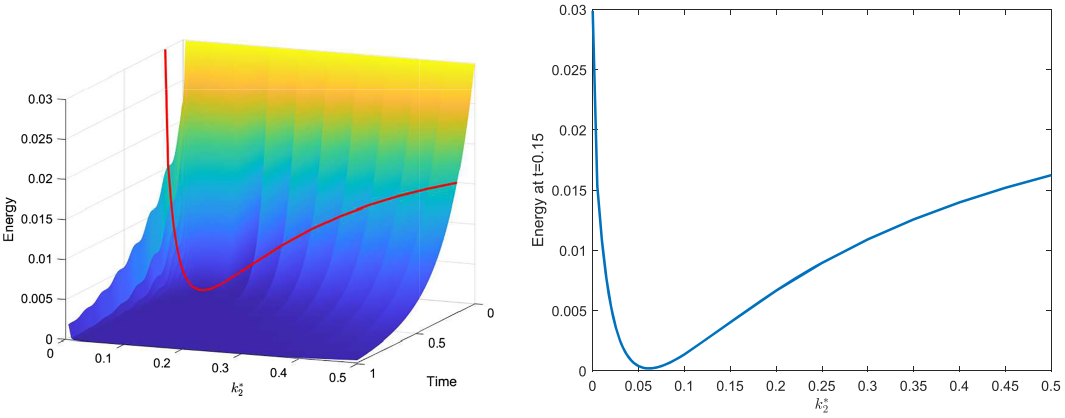


**FIGURE 7** Example 1: energy evolution for different small values of $k_2^*$ [Colour figure can be viewed at wileyonlinelibrary.com]

Therefore, integrating by parts, we derive the following variational formulation for problem (1), (3), and (4).
Find the porosity field $\varphi : [0, T] \to H_0^2(0, \pi)$ such that $\varphi(0) = \varphi_0$, $\dot{\varphi}(0) = \psi_0$, and, for a.e. $t \in (0, T)$ and $r \in H_0^2(0, \pi)$,

$$J(\ddot{\varphi}(t), r) + \delta(\varphi_x(t), r_x) + \delta^*(\dot{\varphi}_x(t), r_x) + k_2(\varphi_{xx}(t), r_{xx}) + k_2^*(\dot{\varphi}_{xx}(t), r_{xx}) + \xi^*(\dot{\varphi}(t), r) + \xi(\varphi(t), r) = 0.$$

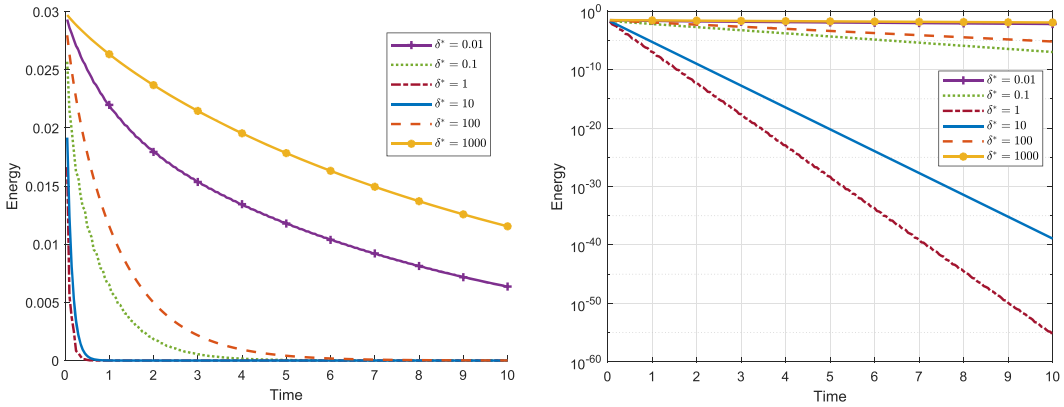


**FIGURE 8** Example 2: dependence of the solution with respect to parameter $\delta^*$ (second-order dissipation mechanism) [Colour figure can be viewed at wileyonlinelibrary.com]

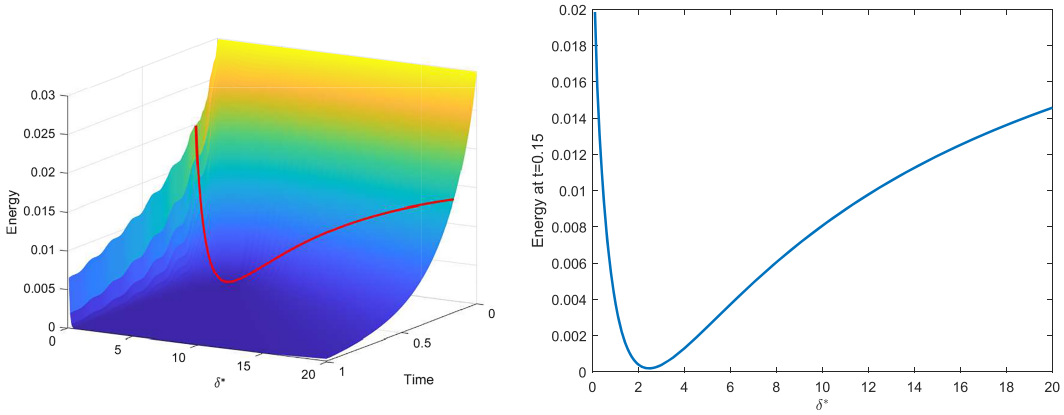


**FIGURE 9** Example 2: energy evolution for different small values of $\delta^*$ [Colour figure can be viewed at wileyonlinelibrary.com]

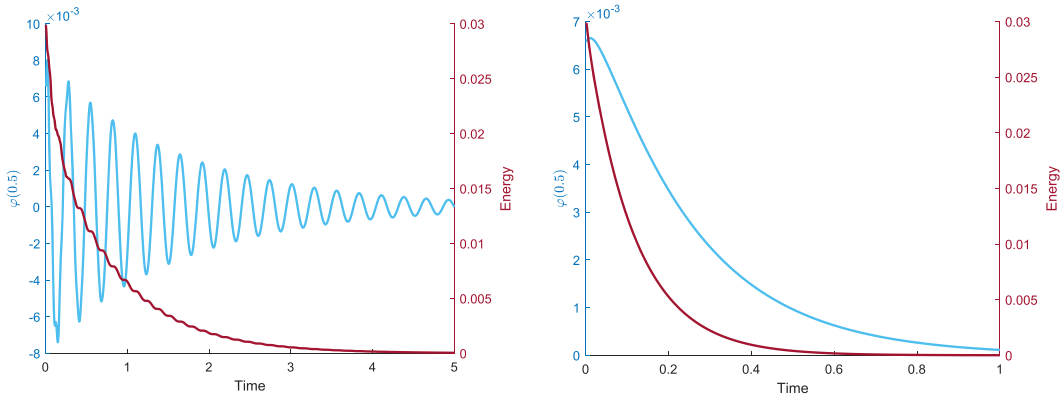


**FIGURE 10** Example 2: energy evolution (red) and porosity (blue) at point $x = 0.5$ for value $\delta^* = 0.01$ (left) and $\delta^* = 10$ (right) [Colour figure can be viewed at wileyonlinelibrary.com]

Now, we provide the fully discrete approximation of the previous weak problem. This is done in two steps. First, we assume that the interval $[0, \pi]$ is divided into $M$ subintervals $a_0 = 0 < a_1 < \ldots < a_M = \pi$ of length $h = a_{i+1} - a_i = \pi/M$, and so, to approximate the variational space $H_0^2(0, \pi)$, we define the finite dimensional space $V^h \subset H_0^2(0, \pi)$ given by

$$V^h = \{e^h \in C^1([0,\pi]) \; ; \; e^h_{|_{[a_i,a_{i+1}]}} \in P_3([a_i, a_{i+1}]) \; i = 0, \ldots, M-1,$$
$$r^h(0) = r^h(\pi) = r^h_x(0) = r^h_x(\pi) = 0\},$$

where $P_3([a_i, a_{i+1}])$ represents the space of polynomials of degree less or equal to three in the subinterval $[a_i, a_{i+1}]$; that is, the finite element space $V^h$ is made of $C^1$ and piecewise cubic functions (Hermite finite elements). Here, $h > 0$ denotes the spatial discretization parameter. Furthermore, let the discrete initial conditions $\phi_0^h$ and $\psi_0^h$ be defined as

$$\phi_0^h = \mathcal{P}^h \phi_0, \ \psi_0^h = \mathcal{P}^h \psi_0,$$

where $\mathcal{P}^h$ is the classical finite element interpolation operator over $V^h$ (see[25]).

Secondly, we consider a uniform partition of the time interval $[0, T]$, denoted by $0 = t_0 < t_1 < \ldots < t_N = T$, with step size $k = T/N$ and nodes $t_n = n\,k$ for $n = 0, 1, \ldots, N$.

Therefore, using the well-known Newmark-$\beta$ scheme,[26] the fully discrete approximations of the above variational problem are the following.

*Find the discrete porosity function* $\varphi^{hk} = \{\varphi_n^{hk}\}_{n=0}^N \subset V^h$ *such that* $\varphi_0^{hk} = \varphi_0^h$, $\psi_0^{hk} = \psi_0^h$ *and, for all* $r^h \in V^h$ *and* $n = 2, \ldots, N$,

$$\begin{aligned}
&\left(\frac{J}{k^2\alpha} + \xi + \xi^* \frac{\beta}{k\alpha}\right)(\varphi_n^{hk}, r^h) + \left(\delta + \delta^* \frac{\beta}{k\alpha}\right)((\varphi_n^{hk})_x, r_x^h) + \left(k_2 + k_2^* \frac{\beta}{k\alpha}\right)((\varphi_n^{hk})_{xx}, r_{xx}^h) \\
&\quad = J\left(\frac{1}{k^2\alpha}\varphi_{n-1}^{hk} + \frac{1}{k\alpha}\dot{\varphi}_{n-1}^{hk} - \left(1 - \frac{1}{2\alpha}\right)\ddot{\varphi}_{n-1}^{hk}, r^h\right) \\
&\qquad + \xi^*\left(\frac{\beta}{k\alpha}\varphi_{n-1}^{hk} + \left(1 - \frac{\beta}{\alpha}\right)\dot{\varphi}_{n-1}^{hk} - k\left(1 - \frac{\beta}{2\alpha}\right)\ddot{\varphi}_{n-1}^{hk}, r^h\right) \\
&\qquad + \delta^*\left(\frac{\beta}{k\alpha}(\varphi_{n-1}^{hk})_x + \left(1 - \frac{\beta}{\alpha}\right)(\dot{\varphi}_{n-1}^{hk})_x - k\left(1 - \frac{\beta}{2\alpha}\right)(\ddot{\varphi}_{n-1}^{hk})_x, r_x^h\right) \\
&\qquad + k_2^*\left(\frac{\beta}{k\alpha}(\varphi_{n-1}^{hk})_{xx} + \left(1 - \frac{\beta}{\alpha}\right)(\dot{\varphi}_{n-1}^{hk})_{xx} - k\left(1 - \frac{\beta}{2\alpha}\right)(\ddot{\varphi}_{n-1}^{hk})_{xx}, r_{xx}^h\right),
\end{aligned}$$

where the discrete porous velocity and the discrete porous acceleration $\dot{\varphi}_n^{hk}$ and $\ddot{\varphi}_n^{hk}$ are now recovered from the relations:

$$\begin{aligned}
\dot{\varphi}_n^{hk} &= \tfrac{\beta}{k\alpha}\varphi_n^{hk} + \tfrac{-\beta}{k\alpha}\varphi_{n-1}^{hk} + \left(1 - \tfrac{\beta}{\alpha}\right)\dot{\varphi}_{n-1}^{hk} + k\left(1 - \tfrac{\beta}{2\alpha}\right)\ddot{\varphi}_{n-1}^{hk}, \\
\ddot{\varphi}_n^{hk} &= \tfrac{1}{k^2\alpha}\varphi_n^{hk} - \tfrac{1}{k^2\alpha}\varphi_{n-1}^{hk} - \tfrac{1}{k\alpha}\dot{\varphi}_{n-1}^{hk} + \left(1 - \tfrac{1}{2\alpha}\right)\ddot{\varphi}_{n-1}^{hk}.
\end{aligned}$$

We note that the first time iteration is done using the central differencing scheme, and so, the discrete porous acceleration at time $t_1$ is obtained as $\ddot{\varphi}_1^{hk} = 4(\varphi_1^{hk} - \varphi_0^h)/k^2 - 4\psi_0^h/k$.

It is straightforward to obtain that this fully discrete problem has a unique solution applying the well-known Lax Milgram lemma and the required assumptions on the constitutive parameters.

In all the numerical simulations described below, we have used the following data:

$$T = 10, \ J = 1, \ k_2 = 1, \ \delta = 2, \ \xi = 2,$$

and the initial conditions, for all $x \in (0, 1)$:

$$\phi_0(x) = x^3(x-1)^3, \ \psi_0(x) = 0.$$

We note that, for the sake of simplicity in the numerical implementation, we have assumed that the length of the beam is 1 (instead of $\pi$). Moreover, we have chosen the discretization parameters $h = 0.025$ and $k = 10^{-3}$ and the Newmark$-\beta$ coefficients $\alpha = 0.25$ and $\beta = 0.5$.

In the first example, we numerically study the dependence of the solution with respect to parameter $k_2^*$ assuming now that $\xi^* = \delta^* = 0$ (i.e., it corresponds to the viscoporosity case). Therefore, the evolution in time of the discrete energy given above is shown in Figure 6 for some values of parameter $k_2^*$ ($k_2^* = 0.1$, 1, 10, 100, 1000) in both natural and semilog scales.

As can be clearly seen, an asymptotic exponential behavior is observed for the discrete energy when $k_2^*$ is less than 100. Although it has been proved theoretically that it should decay as $t^{-1/2}$, we note that this cannot happen in the numerical simulations. This is because, in this case, the variational space has a finite dimension, and so, all the eigenvalues of the corresponding operator (the eigenvalues of the matrix system) have real part. Therefore, the energy decay is always expo-

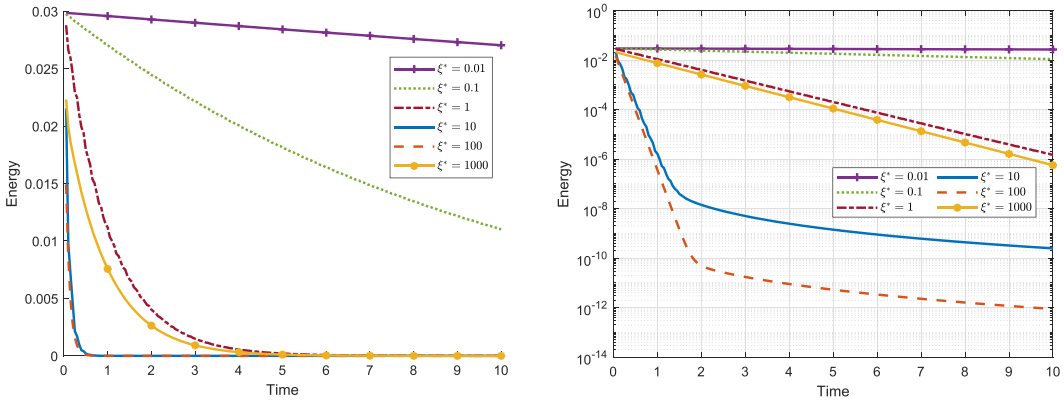


**FIGURE 11** Example 3: dependence of the solution with respect to parameter $\xi^*$ (zeroth-order dissipation mechanism) [Colour figure can be viewed at wileyonlinelibrary.com]

nential. Moreover, we can also appreciate that, when higher values of parameter $k_2^*$ are chosen, the asymptotic behavior degenerates. Even for the largest value $k_2^* = 1000$, the decay is not observed because a much larger final time is needed.

One interesting issue in this experiment is the dependence on parameter $k_2^*$. When it increases, the dissipation mechanism becomes rigid and the energy decay is slower. In Figure 7, we plot the energy decay for a large number of solutions with parameter $k_2^*$ varying between 0.01 and 0.5.

As can be seen on the left-hand side, the energy curve decreases when the parameter $k_2^*$ increases until the value $k_2^* = 0.06$ and then it starts to increase again. In order to analyze easily this behavior, on the right-hand side (and on top of the surface), we plot the values of the energy at time $t = 0.15$, and we can clearly appreciate how this minimum is achieved.

There is a clear difference in the behavior of the system when the dissipation parameter is lower than 0.06 (when we observe the fastest energy decay) and higher than that limit value. These differences will be studied for the next case.

Secondly, we consider the dependence of the solution with respect to parameter $\delta^*$ assuming now that $\xi^* = k_2^* = 0$ (i.e., it corresponds to the hyperviscoporosity case). Thus, the evolution in time of the discrete energy given above is shown in Figure 8 for some values of parameter $\delta^*$ ($\delta^* = 0.01, 0.1, 1, 10, 100, 1000$) in both natural and semilog scales.

As can be seen on the left-hand side, the discrete energy decays exponentially for all the values, including also the greatest values $\delta^* = 100, 1000$, although we observe a clear difference of the behavior for values below $\delta^* = 1$ and higher than $\delta^* = 10$. Hence, we want to analyze in this experiment the dependence on parameter $\delta^*$. When it increases, the dissipation mechanism becomes rigid and the energy decay is slower. In Figure 9, we plot the energy decay for a large number of solutions with parameter $\delta^*$ varying between 0.1 and 20.

As can be seen on the left-hand side, the energy curve decreases when parameter $\delta^*$ increases until value $\delta^* = 2.3$ and then it starts to increase again. As in the previous example, on the right-hand side, we show the values of the energy at time $t = 0.15$ for all the parameters $\delta^*$, and we can easily see that the minimum is found.

Now, to study the different behaviors that appear for low and high values of the dissipation parameter, we study the cases $\delta^* = 0.01$ and $\delta^* = 10$. In Figure 10 we plot the evolution in time of the energy and the porosity at point $x = 0.5$ for these two values. As can be seen, when $\delta^*$ is small, the porosity has strong oscillations and so the energy decay has small perturbations, but when $\delta^*$ is bigger then the oscillations disappear. This occurs because, for low values of the dissipation parameter, the dissipation is not enough to stop the system from oscillating. At a certain value for the parameter, the system is critically damped (in this example for $\delta^* = 2.3$), and the energy dissipation is the fastest possible. After this point, the dissipation is enough to prevent the system from oscillating, but this also reduces its energy dissipation capabilities. Further increasing the dissipation coefficient makes the system too rigid to allow for an efficient dissipation.

Thirdly, we analyze the dependence of the solution with respect to parameter $\xi^*$ assuming now that $k_2^* = \delta^* = 0$ (i.e., it corresponds to the numerical resolution of the weak viscoporosity case). Thus, the evolution in time of the discrete energy is plotted in Figure 11 for some values of parameter $\xi^*$ ($\xi^* = 0.01, 0.1, 1, 10, 100, 1000$) in both natural and semilog scales. In this case, unless for the lowest values $\xi^* = 0.1, 0.01$, the exponential energy decay is clearly achieved (for those values, a very large final time is needed to obtain it). The faster energy decay seems to appear for values between $\xi^* = 10$ and $\xi^* = 100$.

Therefore, we consider now the dependence on parameter $\xi^*$, varying it between 10 and 100. In Figure 12, we plot the energy decay for a large number of solutions, with parameter $\xi^*$ varying between the above commented values $\xi^* = 10$

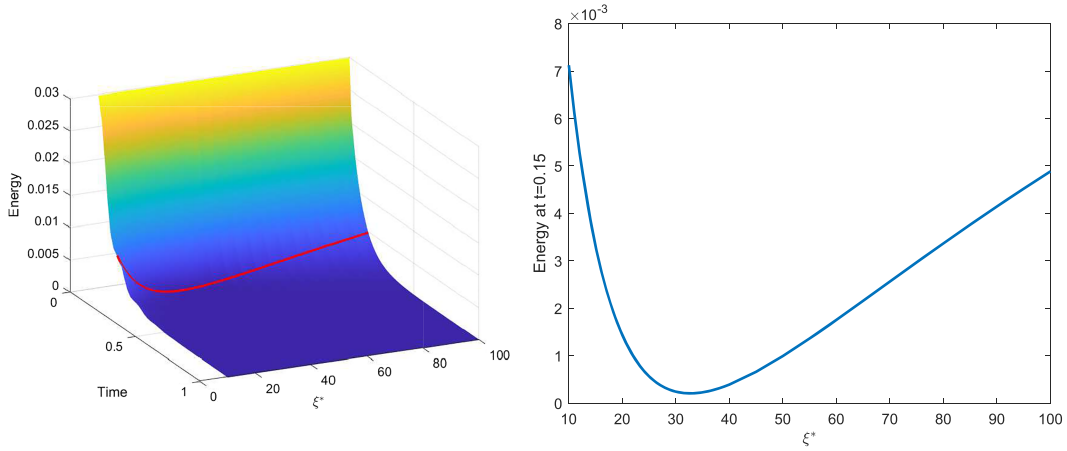


**FIGURE 12** Example 3: energy evolution for different small values of $\xi^*$ [Colour figure can be viewed at wileyonlinelibrary.com]

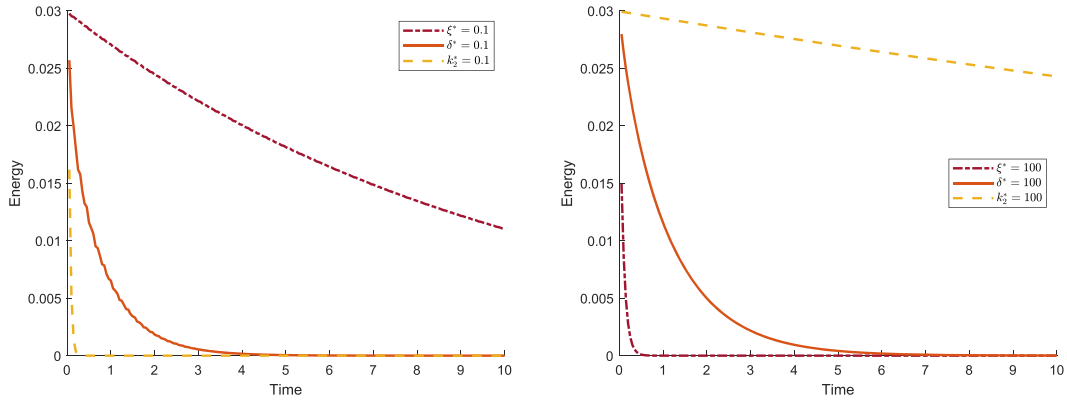


**FIGURE 13** Example 4: comparison among the solutions obtained with the three dissipation mechanism for the cases with values 0.1 and 100 [Colour figure can be viewed at wileyonlinelibrary.com]

and $\xi^* = 100$. On the left-hand side, we can see how the energy decreases at the beginning until the value $\xi^* = 32$ and then it starts to increase. In order to see better how this minimum is reached, we plot the energy at time $t = 0.15$ on the right-hand side.

Finally, the aim is to compare the three dissipation mechanisms with the same values for the equivalent constitutive parameters. The comparison of the energy decays is shown in Figure 13. On the left-hand side, we plot the energy decay taking one parameter equal to 0.1 and the remaining ones equal to zero, meanwhile, on the right-hand side, the energy decay is shown taking one parameter equal to 100 and the remaining ones equal to zero. As can be seen, for small values of the parameters, the best dissipation mechanism is the fourth-order, but when we use large values, the best one is the zeroth-order mechanism. A possible explanation of this behavior is due to the fact that the second-order and fourth-order mechanisms become rigid, and so, the dissipation is worse.

## ACKNOWLEDGEMENTS

This paper is part of the projects PGC2018-096696-B-I00 and PID2019-105118GB-I00, funded by the Spanish Ministry of Science, Innovation and Universities and FEDER A way to make Europe. Funding for open access charge: Universidade de Vigo/CISUG.

## CONFLICT OF INTEREST

The authors declare that they have no conflict of interest.

## ORCID

*Jacobo Baldonedo* https://orcid.org/0000-0002-0377-7208
*José R. Fernández* https://orcid.org/0000-0002-8533-1858
*Ramón Quintanilla* https://orcid.org/0000-0001-7059-7058

## REFERENCES

1. Cowin SC, Nunziato JW. Linear elastic materials with voids. *J Elasticity*. 1983;13:125-147.
2. Cowin SC. The viscoelastic behavior of linear elastic materials with voids. *J Elasticity*. 1985;15:185-191.
3. Nunziato JW, Cowin SC. A nonlinear theory of elastic materials with voids. *Arch Rational Mech Anal*. 1979;72:175-201.
4. Apalara TA. Exponential decay in one-dimensional porous dissipation elasticity. *Q J Mech Appl Math*. 2017;70(4):363-372.
5. Apalara TA. General decay of solutions in one-dimensional porous-elastic system with memory. *J Math Anal Appl*. 2019;469:457-471.
6. Apalara TA. On the stability of porous-elastic system with microtemparatures. *J Thermal Stresses*. 2019;42:265-278.
7. Apalara TA. On the stabilization of a memory-type porous thermoelastic system. *Bul Mal Math Sci Soc*. 2020;43:1433-1448.
8. Baldonedo J, Fernández JR, Magaña A, Quitanilla R. Decay for strain gradient porous elastic waves. Submitted; 2021.
9. Feng B. Uniform decay of energy for a porous thermoelastic system with past history. *Appl Anal*. 2018;97:210-229.
10. Feng B. On the decay rates for a one-dimensional porous elasticity system with past history. *Comm Pure Appl Anal*. 2019;18(6):2905-2921.
11. Feng B, Apalara TA. Optimal decay for a porous elasticity system with memory. *J Math Anal Appl*. 2019;470:1108-1128.
12. Feng B, Yin M. Decay of solutions for one-dimensional porous elasticity system with memory: The case of non-equal waves speed. *Math Mech Solids*. 2019;24:2361-2373.
13. Leseduarte MC, Magaña A, Quintanilla R. On the time decay of solutions in porous-thermo-elasticity of type II. *Discret Cont Dyn Systems Ser B*. 2010;13(2):375-391.
14. Liu Z, Magaña A, Quintanilla R. On the time decay of solutions for non-simple elasticity with voids. *Z Angew Math Mech*. 2016;96(7):857-873.
15. Magaña A, Miranville A, Quintanilla R. Exponential decay of solutions in type II porous-thermo-elasticity with quasi-static microvoids. *J Math Anal Appl*. 2020;492:124504.
16. Messaoudi SA, Fareh A. Exponential decay for linear damped porous thermoelastic systems with second sound. *Discrete Cont Dyn Sys Ser B*. 2015;20:599.
17. Miranville A, Quintanilla R. Exponential stability in type III thermoelasticity with voids. *Appl Math Letters*. 2019;94:30-37.
18. Miranville A, Quintanilla R. Exponential decay in one-dimensional type II thermoviscoelasticity with voids. *J Comput Appl Math*. 2573;368(11):2020.
19. Pamplona PX, Muñoz Rivera JE, Quintanilla R. On the decay of solutions for porous-elastic systems with history. *J Math Anal Appl*. 2011;379:682-705.
20. Pamplona PX, Muñoz Rivera JE, Quintanilla R. Analyticity in porous-thermoelasticity with microtemperatures. *J Math Anal Appl*. 2012;394:645-655.
21. Santos ML, Campelo ADS, Júnior DA. Rates of decay for porous elastic system weakly dissipative. *Acta Appl Math*. 2017;151:1-26.
22. Santos ML, Júnior DA. On porous-elastic system with localized damping. *Z Angew Math Phys*. 2016;67(3):63.
23. Ieşan D. *Thermoelastic Models of Continua*: Springer; 2014.
24. Ieşan D. A gradient theory of porous elastic solids. *Z Angew Math Mech*. 2020;e201900241:100.
25. Ciarlet PG. Basic error estimates for elliptic problems. In: PG Ciarlet, JL Lions, eds. *Handbook of Numerical Analysis*; 1993:17-351.
26. Newmark NM. A method of computation for structural dynamics. *Am Soc Civil Eng*. 1959;85:67-94.

**How to cite this article:** Baldonedo J, Fernández JR, Quintanilla R. Time decay for porosity problems. *Math Meth Appl Sci*. 2021;1-11. doi:10.1002/mma.8054